Available online at www.sciencedirect.com
SCIENCE DIRECT
Earth and Planetary Science Letters 247 (2006) 70–81
EPSL
www.elsevier.com/locate/epsl

Late Oligocene–Early Miocene initiation of shortening in the Southwestern Chinese Tian Shan: Implications for Neogene shortening rate variations

Edward R. Sobel [a,*], Jie Chen [b], Richard V. Heermance [c]

[a] *Institut fuer Geowissenschaften, Universitaet Potsdam, Postfach 601553, 14415 Potsdam, Germany*
[b] *State Key Laboratory of Earthquake Dynamics, Institute of Geology, China Earthquake Administration, P.O. Box 9803, Beijing 100029, P.R. China*
[c] *Department of Earth Science, University of California, Santa Barbara, CA 93106, USA*

Received 11 November 2005; received in revised form 18 March 2006; accepted 30 March 2006
Available online 6 June 2006
Editor: V. Courtillot

Abstract

The Cenozoic Tian Shan is one of the preeminent examples of an intracontinental orogen. However, there remains a significant controversy over when deformation related to the India-Asia collision commenced and therefore how shortening within the mountains has been partitioned over time. One approach has been to look at the modern shortening rate as measured by geodetic studies, combined with estimates of the total shortening across the range and extrapolate backwards. This approach suggests that the onset of range construction was ca. 10 Ma [K.Y. Abdrakhmatov, S.A. Aldazhanov, B.H. Hager, M.W. Hamburger, T.A. Herring, K.B. Kalabaev, K.B. Kalabayev, V.I. Makarov, P. Molnar, S.V. Panasyuk, M.T. Prilepin, R.E. Reilinger, I.S. Sadybakasov, B.J. Souter, Y.A. Trapeznikov, V.Y. Tsurkov, A.V. Zubovich, Relatively recent construction of the Tien Shan inferred from GPS measurements of present-day crustal deformation rates, Nature 384 (6608) (1996) 450–453]. An alternate method is to determine the age of the onset of exhumation using thermochronology. We present 19 new apatite fission-track (AFT) results from the southwestern Chinese portion of the belt; this region represents the first area exhumed during the late Tertiary along a transect at ca. 76°E. Exhumation commenced at the Oligocene–Miocene boundary (~ 24 Ma) along the Maidan and Muziduke thrusts, which bound the southern side of the Kokshaal range. Subsequently, deformation propagated ca. 20 km south to the Kashi basin-bounding thrust (KBT), which was exhumed by no earlier than 18.9±3.3 Ma. Three detrital AFT samples from Plio-Pleistocene strata deposited ca. 20 km farther south contain fission track grain age peaks that young monotonically upwards from 20.9+7.0/− 5.3 Ma to 15.9+5.4/− 4.0 Ma with a fairly constant lag time of 16 to 18 Ma. These ages, combined with structural data, suggest that both the hanging wall and the footwall of the KBT experienced a renewed episode of exhumation during the latest Cenozoic. The discrepancy between the Late Oligocene–Miocene initiation of significant exhumation shown herein and the 10 Ma initiation estimate from geodesy suggests that the Tian Shan has undergone a complex Late Cenozoic shortening history. Assuming that the present shortening rate could account for the total amount of Cenozoic shortening in 10 Ma and realizing that shortening initiated at least 15 Myr earlier, we conclude that the shortening rate must have varied over time, possibly in pulsed-southward migrating events, and that the present rate may not reflect the average rate since initiation of range uplift.

Keywords: Tian Shan; fission track; thermochronology; Cenozoic; deformation

* Corresponding author. Fax: +49 331 977 5700.
E-mail address: sobel@rz.uni-potsdam.de (E.R. Sobel).

0012-821X/$ - see front matter © 2006 Elsevier B.V. All rights reserved.
doi:10.1016/j.epsl.2006.03.048

1. Introduction

The 2500 km long Tian Shan comprise the most significant Central Asian topography north of the Tibetan Plateau, with several peaks exceeding 7000 m. Situated between the enormous Tarim basin to the south and the Chu and Junggar basins to the north (Fig. 1), this region forms one of the world's best expressed intracontinental mountain belts. Deformation is driven by the active continental collision between India and Asia, located up to 1500 km to the south. We focus on the portion of the range between the Talas Ferghana fault and the region with the highest peaks: the Kyrgyz Central Tian Shan and the Chinese Western Tian Shan. There, the present-day structure of the reverse- and thrust-fault bounded Tian Shan consists of roughly E–W-trending ranges separated by roughly parallel thick late Cenozoic sedimentary basins (e.g., [1]). At present, dominantly contractile seismicity and deformation are distributed across the width of the orogen (e.g., [2–4]) and geodetic studies document a continuous gradient of shortening between Kashgar and Bishkek [5,6].

Although present-day deformation is evenly distributed, the early stages of range growth are poorly constrained. Key questions are when and where this shortening commenced. One approach has been to look at the modern shortening rate as measured by geodetic studies [5–7], estimates of the total shortening across the range [8], and extrapolate backwards. Modern shortening rates across the entire range are estimated to be 19±3 mm/yr at 76°E (Fig. 1). This value [5,6] comprises a significant proportion of the present geodetically-determined India-Eurasia convergence rate of 35 mm/yr (REVEL, [9]). Avouac et. al. [8] estimated 203±50 km of shortening across 76°E longitude based on area-balancing of the assumed crustal thickening under the mountain belt and adding

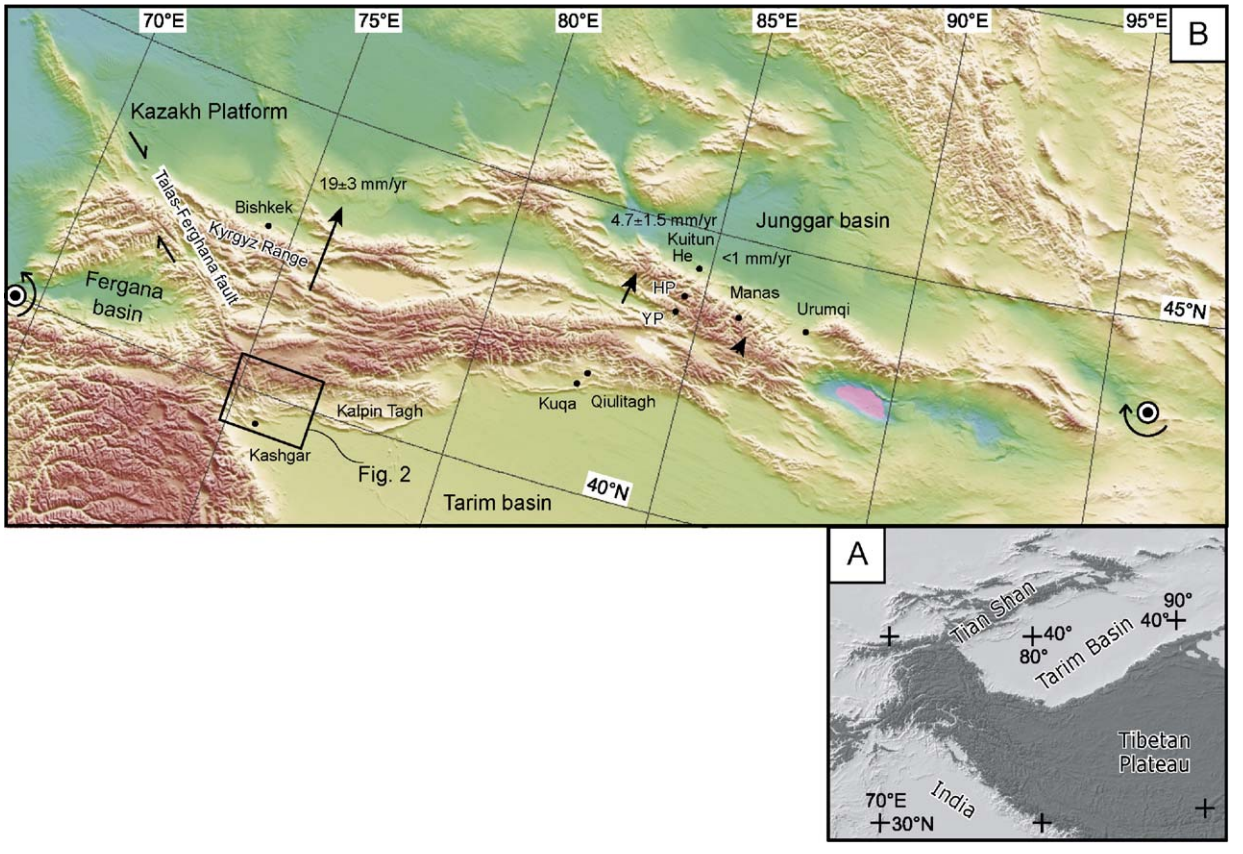

Fig. 1. (A) Topographic map of central Asia, showing locations of the Tian Shan with respect to adjacent plateaus and basins. (B) Topography of the Tian Shan derived from GTOPO30 digital elevation model. Shortening in the Tian Shan has been linked with 7±2.5° clockwise rotation of the Tarim block about the pivot point shown at 96°E [8]. The Ferghana basin has rotated counterclockwise 26°±7° about the pivot shown at ~ 70°E [51]. Arrows and rates (mm/yr) denote GPS-derived estimates for the present shortening rate across the range [5–7]. HP is Haxilegen Pass; YP is Yuximelegai Pass. Kashi is also known as Kashgar.

sediment lost by erosion, taking into account the isostatic response. Using 200 km of shortening and 20 mm/yr deformation rate, this approach suggests that the onset of range construction was ca. 10 Ma [5]. While much of the GPS data have been collected in the Kyrgyz Tian Shan, the majority of the geological evidence has been obtained from regions ca. 500 km to the east. This raises the possibility that the onset of shortening could vary along strike within the Tian Shan.

A traditional method for determining the onset of shortening is to examine the sediments stored in the adjacent foreland basin. The Tarim and Junggar basins lie on the south and north sides of the Tian Shan, respectively. Unfortunately, non-marine Oligo-Miocene stratigraphy from these basins has poor biostratigraphic resolution and a complete absence of volcanic ashes, making accurate stratigraphic age determinations difficult. Yin et al. [10] proposed an Early Miocene age of shortening based on rough magnetostratigraphic dating of the onset of conglomerate deposition in the Kuqa region; however, a new, higher resolution magnetostratigraphic data for this section (the Qiulitagh anticline) yields a Middle to Late Miocene age for this conglomerate [11]. Indeed, magnetostratigraphic studies in the Kashi Basin show that prominent range-bounding conglomerates are time-transgressive [12–14]; therefore, the onset of more rapid exhumation and/or more proximal thrusting could have started even earlier than any single age reported from a basin. Based on an evaluation of mass accumulation in these basins, Métivier and Gaudemer [15] suggested that the onset of shortening was ca. 16 Ma, although the underlying stratigraphic resolution can be debated. Reflection seismic data from the subsurface south of Kuqa shows an angular unconformity above the late Oligocene Suweiyi Formation [16], indicating that the onset of deformation at this locality (slightly) post-dates this time.

Alternatively, one can examine thermochronologic data to constrain the onset of cooling. We assume that this cooling is linked with exhumation driven by crustal shortening, although cooling may lag behind the onset of deformation (e.g., [17] and references therein). Apatite fission-track cooling ages from a vertical profile along the north flank of the Tian Shan adjacent to the Junggar Basin, near Manas, and from detrital grains deposited in Miocene sandstones from the NW Tarim basin suggest that shortening commenced around the Oligocene–Miocene boundary [18,19].

Using apatite fission-track thermochronology, we have studied the cooling history of every major topographic range along a transect between Kashgar and Bishkek ([19–21], Sobel, unpublished); in this study, we report on the area hosting the oldest Cenozoic results. These data constrain the onset of exhumation along the southern flank of the Tian Shan at 76°E. In turn, we address whether the shortening rate has varied since the onset of deformation.

2. Geologic setting

The Tian Shan records a complex Paleozoic history of island arc accretion (e.g., [22,23]). The final ocean closure occurred in the Late Carboniferous–Early Permian, represented by ophiolites and eclogite in the Atbashi range in southern Kyrgyzstan, ca. 100 km north of our study area [24,25]. Suturing was followed by Permian orogen-parallel strike-slip deformation (e.g., [26,27]). Although episodes of intracontinental deformation driven by distal plate margin tectonism occurred during the Early–Middle Jurassic and the Late Jurassic–Cretaceous (e.g., [28]), in the immediate study area, Mesozoic tectonism resulted in little measurable exhumation [19,20].

The deformation style of the study area is illustrated by a geologic map and cross-section from the Kokshaal range south to the Tarim basin (Fig. 2). The cross-section cannot be balanced because hanging-wall cutoffs have been eroded, one fault is poorly exposed, and some faults are parallel to bedding. From north to south, the region is characterized by three main kinematic elements: (1) two major south-vergent faults bounding the range that represent the Cenozoic reactivation of a late Paleozoic thrust system [29]. The northernmost, the South Tian Shan Fault, can be traced eastwards for over 850 km [30]; both footwall and hanging-wall units are comprised of Paleozoic sediments. In the study area, this fault is known as the Maidan fault; we use this name herein. The Maidan fault appears to be kinematically-linked with the Talas-Ferghana dextral fault to the west, which has had 60±10 km of Late Cenozoic dextral slip [31]. South of the Maidan fault lies a narrow belt of folded Paleozoic units that is in turn bounded on the south by the Muziduke fault. This thrust fault is well defined ca. 40–50 km along strike to the east [32,29]. However, in our study area, extensive Quaternary deposits obscure the fault (compare Fig. 2A and B). Detailed geological maps of the Kokshaal range north of the Maidan fault are unavailable and we were unable to visit this region due to the proximity of the international border; however, no major faults are reported from this region. In addition, a late Cretaceous regional erosion surface is preserved on the north flank of the range, ca. 20 km north of the fault (Fig. 2A), implying that there

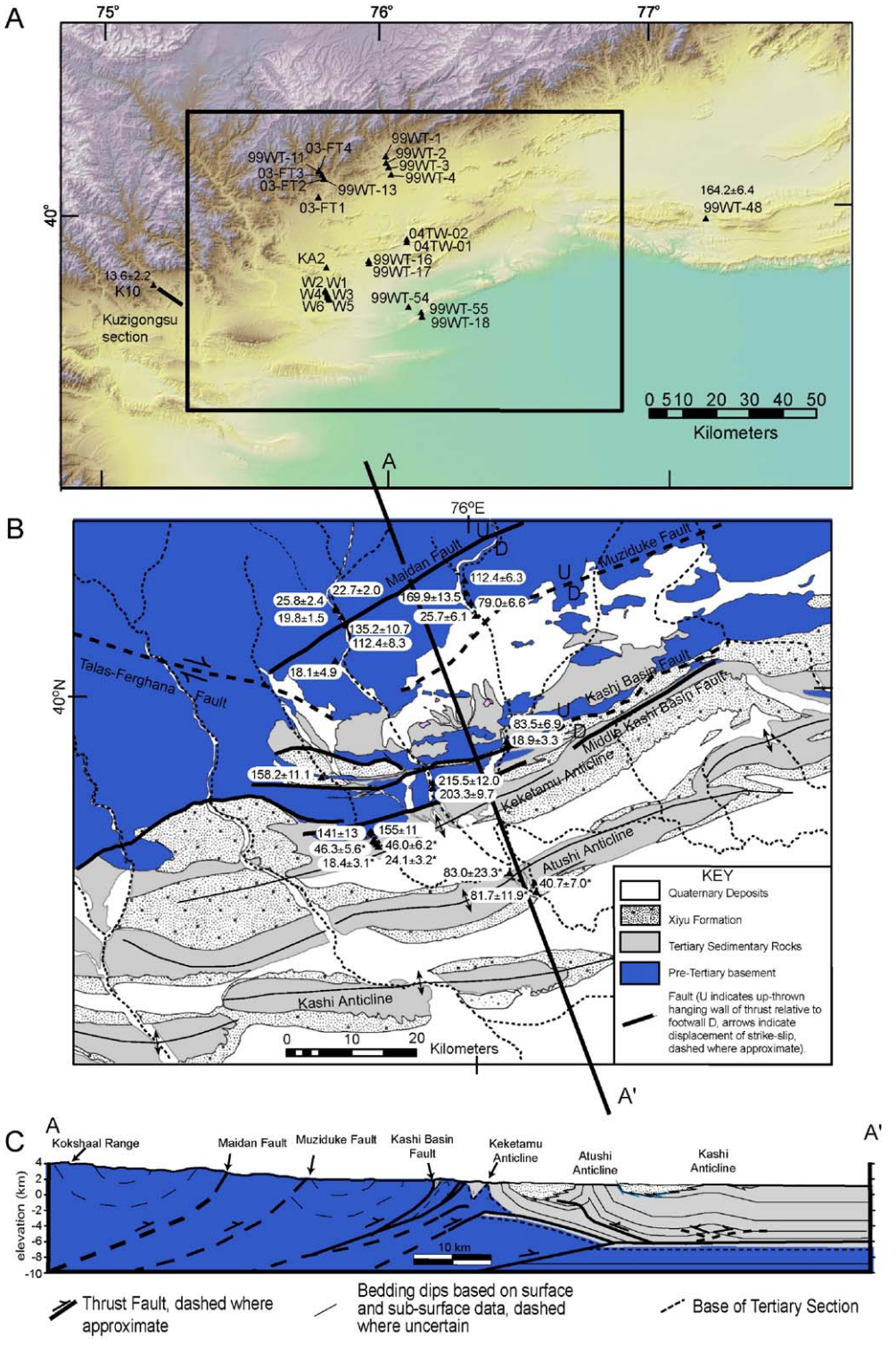

Fig. 2. (A) Shaded relief 90 m digital elevation model of the study area, showing sample locations. Rectangle marks location of (B). Samples W1–W6 are from the Wenguri locality [19]; data are presented in Tables 1 and 2. Sample K10 is from the Kuzigongsu locality [19]; this is the youngest, reset component from a stratigraphic sequence of 10 samples. (B) Geological map of the study area, modified from Scharer et al. [50] and unpublished work by Heermance and Chen. Apatite fission-track ages shown correspond to sample numbers in (A). Ages with * are detrital samples. A–A′ shows the location of the cross-section shown in (C). (C) Cross-section through the study area, showing major faults.

are no major, datable Cenozoic structures in that region. (2) The Kashi Foreland Basin is ~ 160 km long by 70 km wide. The basement Paleozoic series is thicker and better exposed in the Kalpin Tagh thrust belt, ca. 50 km along strike to the east. Lower Cretaceous fine-grained sandstones and thin (<50 m thick) Paleogene shallow marine deposits unconformably overlie the Permian in the southwestern part of the study area; these pinch out to the east [33]. Although thick Jurassic strata outcrop to the west of the Talas-Ferghana fault, they are absent in the study area. A 6- to 10-km-thick sequence of late Early Miocene and younger strata paraconformably overlies the Cretaceous and Paleogene deposits. The northern basin margin is defined by the Kashi basin-bounding thrust fault (KBT), which places Paleozoic strata over Tertiary conglomerates. The KBT fault is now upright and overturned, suggesting that a younger fault further south, the Middle Kashi basin thrust fault (MKBT, also called the Kepingtagh-Tashipisake fault), has uplifted and deformed both the hanging wall and the footwall of this structure. The structural style changes from north to south, varying from an imbricated thrust stack (KBT and MKBT, where slices of Paleozoic strata making up the former Tarim platform are thrust south toward the basin) and associated fault-related folds (Keketamu anticline pairs) in the northern part of the basin, to distinctive Quaternary detachment folds (Atushi-Talanghe fold, Kashi-Mingyaole fold) along the southern front of the fold-and-thrust belt (Fig. 2B). The wavelength of the major structures within the Kashi basin varies from 5 to 10 km, with the shorter wavelengths corresponding to structures with greater shortening magnitude. Palinspastic reconstructions across the basin indicate that >20 km of shortening is accommodated on these five major structures [34]. The age of the Tertiary sediments is constrained by magnetostratigraphy throughout the basin. Deformation in the medial basin at the Keketamu anticline initiated between 4.5 and 5.0 Ma, based on the age of growth strata. Further north in the “proximal” basin adjacent to the KBT fault, syn-tectonic Tertiary stratigraphy is potentially as old as 18 Ma [14]. Detachment folding in the distal (southern) basin began recently at 2 Ma, based on the age of growth strata [12,35]. These ages indicate that deformation has been progressing southward into the Kashi basin since the onset of basin formation. (3) The Tarim craton, with little internal deformation, dips gently northwest below the sediment-filled Kashi foreland basin.

Apatite fission-track (AFT) data from an over 6 km thick composite section of Precambrian through Permian strata in the eastern Kalpin Tagh document a strong late Paleozoic exhumation event [20]. Track length modeling combined with stratigraphic analysis suggests ca. 5 km of exhumation commenced at ca. 250±10 Ma. Permian exhumation was apparently driven by the collision between the Tarim-South Tian Shan and the Central Tian Shan blocks [20]. This exhumation event apparently affected our study area as well, providing a general AFT reference age.

Two Cretaceous and four Miocene fine-grained sandstones from the Wenguri section were previously analyzed for AFT [19,20]; the data are listed in Table 1. The Cretaceous samples yielded detrital ages of 141±13 and 155±11 Ma; modeling yielded provenance ages of 160–260 Ma that were subjected to maximum Cenozoic burial temperatures of 80–90 °C. The basal age of the Cenozoic strata has been refined to ca. 18 Ma based on magnetostratigraphy [14]. All of the overlying samples contain three age components. The oldest is similar to the Cretaceous samples; the youngest generally youngs upsection, with ages of 23.5±3.9, 25.0±3.9, 16.9±2.7 and 13.1±2.2 Ma (Table 2). Mean track length generally increases upsection, suggesting that Cenozoic heating was caused by burial beneath late Cenozoic strata, and possibly also by south-vergent overthrusting by the KBT and MKBT. The Oligo-Miocene ages are interpreted as reflecting the onset of exhumation in the South Tian Shan; however, the source area for the sediments could not be determined [19]. Younger thrusting has propagated southward into the Tarim basin. This is documented by exhumation of the thick Kuzigongsu section at 13.6±2.2 Ma along a south-vergent thrust located south of the section (Fig. 2A) [19].

3. Fission-track methodology

The study area is characterized by thrusts and folds, suggesting that exhumation driven by contractile deformation and erosion is the primary mechanism for late Cenozoic cooling. In this setting, apatite fission-track cooling ages from rocks that have been exhumed from above the total annealing temperature can provide a close approximation of the deformation age (e.g., [36]). For moderately rapidly cooled (10 °C/Ma) apatites with between 0.03 and 0.10 wt.% Cl, typical of this study, the total annealing temperature is ~ 105 to 110 °C [37]. Samples that were above the total annealing isotherm prior to Cenozoic exhumation resided in the (now exhumed) partial annealing zone (PAZ) for some period of time and therefore have ages reflecting the penultimate cooling event, (strongly) modified by partial annealing (e.g., [21]). In this study, partially reset samples have Cretaceous and older ages

Table 1
Apatite fission-track data

Sample	Litho. age	N lat. (deg.)	E long. (deg.)	Elevation (m)	No Xls	NS	Rho-S ($\times 10^6$)	NI	Rho-I ($\times 10^6$)	ND	Rho-D ($\times 10^6$)	$P(\chi^2)$ (%)	Age (Ma)	$\pm 1\sigma$ error	U (ppm)	Zeta	Cl (wt.%)	Stdev.	Length (μm)	Error (μm)	Stdev. (μm)	No. length	Etch
Hanging wall of Maidan fault																							
03-FT4	C	40.1216	75.7686	2579	17	149	0.3701	1482	3.6810	4938	1.2253	96	22.7	2.0	38	370			13.58			1	C
99WT-11	C	40.1189	75.7697	2637	23	203	2.5120	1568	1.9400	7204	1.1080	33	25.8	2.4	22	361	0.04	0.07	13.49	0.35	0.77	5	B
03-FT3	C	40.1096	75.7793	2552	32	224	0.2938	2562	3.3600	4938	1.2296	55	19.8	1.5	34	370			12.61	1.87	4.19	5	C
Hanging wall of Muziduke fault																							
03-FT2	C	40.0988	75.7847	2544	21	442	0.7871	733	1.3050	4938	1.2339	4	*135.2*	*10.7*	13	370			11.21	0.80	2.41	9	C
99WT-13	C	40.0978	75.7878	2540	20	906	0.9368	1459	1.5090	7204	1.1160	0	*112.4*	*8.3*	17	361	0.09	0.15	10.98	0.37	2.43	43	A
99WT-1	C	40.1581	76.0036	2400	14	620	1.1860	1085	2.0760	7204	1.0730	6	112.4	6.3	24	361	0.04	0.07	12.00	0.36	2.13	36	B
99WT-2	C	40.1406	76.0061	2350	19	612	1.3050	694	1.4800	7204	1.0820	20	169.9	13.5	17	361	0.02	0.04	9.47	0.81	3.52	19	A
99WT-3	C	40.1275	76.0139	2325	23	544	1.5540	1464	4.1830	7204	1.0900	0	*79.0*	*6.6*	48	361	0.10	0.12	11.10	0.30	2.51	71	A
99WT-4	C	40.1089	76.0228	2255	6	20	1.7110	158	1.3520	7204	1.0990	68	25.7	6.1	15	361	0.03	0.02	12.10	1.40	2.40	3	A
03-FT1	C	40.0480	75.7665	2392	8	15	0.1465	189	1.8460	4938	1.2382	5	*18.1*	*4.9*	19	370			10.14			1	C
Hanging wall of KBT fault																							
04TW-02	Pz (P?)	39.9328	76.0757	1740	20	519	0.7898	1252	1.905	4566	1.0841	1	*83.5*	*6.9*	22	370			12.36	0.25	1.99	61	D
04TW-01	Pz (P?)	39.9253	76.0758	1740	14	36	0.1227	382	1.302	4566	1.0893	66	18.9	3.3	15	370							D
Footwall of KBT fault																							
99WT-16	P	39.8761	75.9414	1930	20	1315	2.4930	1194	2.2640	7204	1.1250	2	*215.5*	*12.0*	25	361	0.09	0.11	12.31	0.17	1.72	100	B
99WT-17	P	39.8689	75.9414	1933	19	1151	2.3059	1167	2.3380	7204	1.1331	85	203.3	9.7	26	370			12.02	0.26	1.62	106	A
KA2	K	39.8583	75.792	1950	14	882	1.528	1292	2.2390	5291	1.2883	0	*158.2*	*11.1*	22	370			12.55	0.22	1.64	53	C
Footwall of MKBT; Wenguri section (from Sobel and Dumitru, 1997)																							
W6	K	39.7958	75.7867	1880	20	990	1.729	1621	2.831	6447	1.457	<0.1	*155.0*	*11.0*	29	361			10.92	0.16	1.64	100	E
W5	K				19	718	0.824	1396	1.603	4609	1.571	< 0.1	*141.0*	*13.0*	14	386			11.51	0.15	1.45	100	E
W4	Mio				40	953	1.068	5383	6.032	6447	1.452	<0.1	*46.0*	*6.2*	57	361			11.71	0.18	1.78	101	E
W3	Mio	39.7917	75.7892	1880	50	1703	1.171	10,223	7.03	6447	1.452	<0.1	*46.3*	*5.6*	61	361			11.66	0.18	1.82	100	E
W2	Mio				32	569	1.057	6923	12.85	6447	1.448	<0.1	*24.1*	*3.2*	130	361			12.71	0.19	1.93	100	E
W1	Mio				32	449	0.64	7087	10.1	4609	1.565	<0.1	*18.4*	*3.1*	90	361			13.24			41	E
Kalpin Tagh																							
99WT-48	D	39.9739	77.1258	1750	18	1818	1.6710	2444	2.2460	7204	1.2100	21	164.2	6.4	23	361	0.10	0.12	11.85	0.18	1.96	125	B
Boguzihe magnetostratigraphic section																							
99WT-54	modern	39.7492	76.0781	1440	18	675	0.5833	1256	1.0850	7204	1.2270	0	*83.0*	*23.3*	11	361			12.87	0.24	1.47	38	B
99WT-18	Plio; top	39.7225	76.1258	1380	34	503	0.2762	2400	1.3180	7204	1.1420	0	*40.7*	*7.0*	14	361			13.33	0.28	1.65	34	B
99WT-55	Plio; base	39.7347	76.1228	1370	37	1819	0.9481	4558	2.3760	7204	1.2350	0	*81.7*	*11.9*	24	361	0.05	0.11	12.57	0.18	1.64	81	B

Age: D is Devonian, C is Carboniferous, P is Permian, K is Cretaceous, Mio is Miocene, Plio is Pliocene, No Xls, number of individual grains dated per sample; NS, number of spontaneous tracks counted; Rho-S, spontaneous track density; NI, number of induced tracks counted; Rho-I, induced track density in external detector; ND, number of tracks counted in determining Rho-D; Rho-D, induced track density in external detector adjacent to CN-5 dosimetry glass; $P(\chi^2)$ (%), chi-square probability. Samples analyzed following the procedures described in [17]. All apatites from this study were etched with 5.5 mol nitric acid. (A) 20 s, 23 °C; (B) 23 s, 23 °C; (C) 20 s, 20.9 °C; (D) 20 s, 21.0 °C; (E) 5.0 mol nitric acid, 20 s, room temperature. Samples were irradiated at Oregon State University. Following irradiation, the mica external detectors were etched with 21 °C, 40% hydrofluoric acid for 45 min. The pooled (*central*) age is reported for samples that pass (fail) the χ^2 test [38,39]; error is one sigma, calculated using the zeta calibration method [52] with zeta of 361±20 or 369.6±7.6 for apatite (E. Sobel, unpublished) for samples analyzed prior to or after mid-2002, respectively. Wenguri samples calculated with zeta of 361.5 (E. Sobel, unpublished, 1993) or 385.9 (T. Dumitru, unpublished, 1993).

Table 2
Apatite fission-track grain age components

Sample	Dep. age (Ma)	No. grains	No. pops	pop 1 D1	− Error	+ Error	pop2 D2	− Error	+ Error	pop3 D3	− Error	+ Error	pop4 D4	− Error	+ Error
Boguzihe section															
99WT-54	0	18	2	15.9	4.0	5.4				255.2	29.2	32.8			
% of sample				60.7						39.3					
99WT-18	1.7	34	3	19.0	4.0	5.1	67.4	10.6	12.6	299.2	132.9	234.7			
% of sample				52.7			43.8			3.5					
99WT-55	3.0	37	3	20.9	5.3	7.0	43.8	7.4	8.9	166.2	20.1	22.8			
% of sample				31.3			22.0			46.7					
Wenguri section, from [19]															
W1	<18	41	3	13.11	2.17	2.17	33.48	4.26	4.26	134.41	21.05	21.05			
% of sample				84			13			3					
W2	<18	100	3	16.94	2.72	2.72	40.57	6.67	6.67	99.75	12.68	12.68			
% of sample				82			12			7					
W3	<18	100	3	25.01	3.88	3.88				104.12	5.49	5.49	180.2	18.37	18.37
% of sample				73						21			6		
W4	18	101	3	23.53	3.89	3.89	51.78	3.98	3.98	146.95	10.62	10.62			
% of sample				57			27			16					

All errors are ±95% CE. Population ages and errors are in Ma. Boguzihe components calculated using the BINOMFIT program [42]; see text for details. Wenguri data are taken from [19]. Different populations in the two sections are not necessarily correlated; i.e., D2 Boguzihe may correspond to a different source than D2 Wenguri.

and shortened track length distributions while reset samples have Late Oligocene to Miocene ages.

Sample preparation and analytical details follow [17]; additional details are presented in Table 1. All analytical results are presented in Fig. DR1 in Appendix A. Many samples yielded only small amounts of apatite. The young apatite samples provided very few horizontal confined track-length measurements; up to 125 track lengths were measured from older samples. The pooled (central) age is reported for samples that pass (fail) the χ^2 test [38,39], indicating a concordant (discordant) population of grains. To assess the Cl content of the apatite [40], nine samples were analyzed with a CAMECA SX-100 electron microprobe (Table 1). For these samples, every crystal with a single grain age or a confined track-length measurement was probed. Although some samples have multiple compositions, virtually all grains have wt.% Cl between 0.00 and 0.20 (Fig. DR1 in Appendix A).

4. Results

Two sampling transects were collected across the southern margin of the range (Figs. 2 and DR1 in Appendix A; Table 1). Together, these samples are from both the South Tian Shan (Maidan) and the Muziduke faults. Three apatite-bearing samples were collected from the hanging wall of the Maidan fault along the western transect. Samples 99WT-11 and 03-FT4 are about 2.4–2.7 km north of the fault and have ages of 25.8±2.4 and 22.7±2.0 Ma, respectively; sample 03-FT3 is located 1.1 km from the fault and has an age of 19.8±1.5 Ma. Samples from the footwall of the Maidan fault yield Mesozoic ages close to the Maidan fault and Miocene ages adjacent to the Muziduke fault. The Mesozoic samples have shortened track-length distributions. The youngest of these, 99WT-3, is about 7 km SSE of the fault and has an age of 79.0±6.6 Ma, a mean track length of 11.10±0.30 μm, and multicompositional apatite with a mean of 0.10 wt.% Cl. Only 71 confined track lengths could be measured, sufficient for modeling with moderate resolution. Modeling using the AFT-Solve program [41] suggests that the sample experienced 20 to 52 °C of Miocene reheating followed by Miocene or Pliocene exhumation (Fig. 3). Reheating was likely caused by burial beneath either the hanging wall of the Maidan thrust or sediment eroded from the thrust; this burial heating significantly reduced the apparent age of the sample. The two southernmost samples, 99WT-4 and 03-FT1, have ages of 25.7±6.1 and 18.1±4.9 Ma, respectively; the younger of these fails the chi-squared test. These two samples are just north of the south-vergent Muziduke fault.

Unfortunately, exposures of Paleozoic strata immediately to the south of the Muziduke fault are sparse. Two Permian sandstone samples were analyzed from the hanging wall of the KBT. The southern, 04TW-01, yielded a pooled age of 18.9±3.3 Ma; the northern,

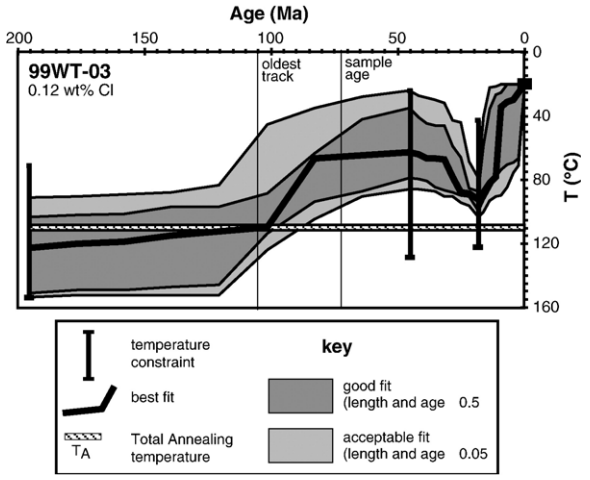

Fig. 3. Representative AFTSolve track-length model for sample 99WT-3, using the dominant apatite composition of 0.12 wt.% Cl. Models were run with 4 constraints. Models were started at 195 Ma, with a temperature range between 70 and 155 °C, such that all tracks initially formed could be completely annealed. The next constraint at 45 Ma (24–128 °C) postdates formation of the regional erosion surface. The observed shortened track-length distributions require a late-stage heating event such as might be caused by burial beneath a sedimentary basin. Nine runs were made, with the onset of modeled cooling shifted stepwise between 19 and 4 Ma. At this time, the model permitted sample temperatures between 43 °C and 122 °C. Acceptable fits were not limited by the temperature or the position of the constraints, with the exception of the age of final cooling. Temperature paths between adjacent constraints had 8 segments. Heating and cooling rates were not constrained. Each model run had 10,000 iterations, using a Monte Carlo approach. Models cannot constrain the time of the final cooling event; however, they provide good constraints on the magnitude of this cooling. The average maximum reheating temperature was ca. 90 °C (best fit)±ca. 10 °C (good fits); average reheating temperature was ca. 38 °C (best fit)+14/− 18 °C (good fits). The total annealing temperature for this sample history is ca. 110 °C.

04TW-02, yielded a central age of 83.5±6.9 Ma. These samples are 0.1 and 0.8 km north of the KBT fault, respectively. Apparently the amount of exhumation decreases north away from the fault, such that the nearer sample was exhumed from depths below the total annealing isotherm while the farther sample was exhumed from a position within the partial annealing zone. This is a likely scenario because 04TW-01 would have been stratigraphically below the KBT at the initiation of exhumation but has since been exhumed through the PAZ and rotated along with the KBT in the hanging wall of the MKBT, so now both the KBT and Paleozoic strata are overturned at this locality.

A group of samples were analyzed from the footwall of the KBT. Two Permian sandstone samples ~ 2.5 km south of the fault yielded a central age of 215±12 Ma with a mean track length of 12.31±0.17 μm (99WT-16) and a pooled age of 203.3±9.7 Ma with a mean track length of 12.02±0.26 μm (99WT-17). A Devonian sandstone 90 km to the east, on the western margin of the Kalpin Tagh, yielded an age of 164±6 Ma and a mean track length of 11.85±0.18 μm (99WT-48). These results are generally compatible with the thermal history determined for the Kalpin Tagh by Dumitru et al. [20], suggesting that the study area experienced a strong exhumation event that commenced during the latest Paleozoic or earliest Mesozoic. A Cretaceous sandstone sample, KA2, yielded a central age of 158±11 Ma and a mean track length of 12.55±0.22 μm; quite similar to results from Cretaceous sandstones sampled at the Wenguri section, 7 km to the south, reported by Sobel and Dumitru [19]. The Cretaceous sandstones were apparently sourced from adjacent Paleozoic units [19].

Samples 99WT-55, 99WT-18, 99WT-54 were analyzed from the Boguzihe paleomagnetic stratigraphic section from the Atushi-Talanghe anticline, with depositional ages of 3.0, 1.7, and 0 (modern) Ma [12], respectively. Fission Track Grain Age components (FTGA) were determined using BINOMFIT [42] and are shown in Table 2. Examination of these components suggests that they belong to 3 discrete age groups,

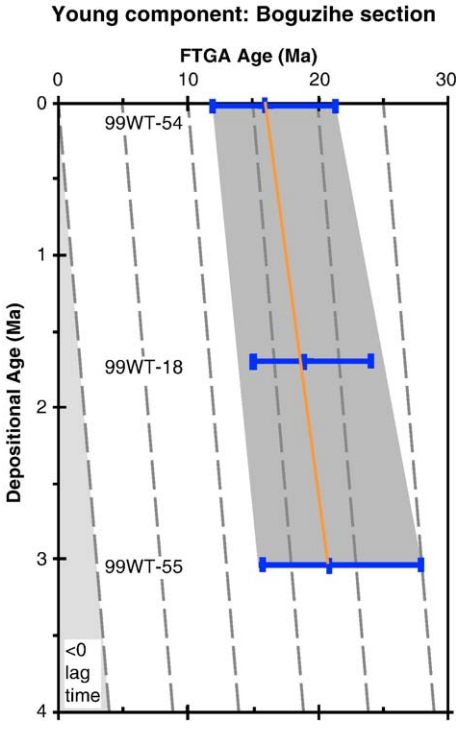

Fig. 4. Lag time plot for the Boguzihe section. Depositional ages are based on paleomagnetic stratigraphy [12]. Dashed grey lines show constant lag time. Only the youngest fission-track grain age component is shown here; the full data set is shown in the data repository. Data are presented in Table 2.

labeled D1, D2 and D3. Although relatively few apatite crystals could be counted, the youngest component of the three samples reveals a clear trend. This D1 detrital path has ages that young monotonically upwards from 20.9+7.0/− 5.3 Ma to 19.0+5.1/− 4.0 Ma to 15.9+5.4/− 4.0 Ma and has a fairly constant lag time of 16 to 18 Ma (Fig. 4). Although the onset of exhumation in the source area cannot be defined from this data, the ages are similar to those sampled from outcrops in the Kokshaal range. The source area represented by the D2 path (43.8+8.9/− 7.4 and 67.4+12.6/− 10.6 Ma; Table 2) has not yet been identified in the landscape; the lack of known tectonism of this age suggests that the grains were sourced from an exhumed partial annealing zone that formerly overlay either the Kokshaal range or the hanging wall of the KBT. The ages comprising the D3 path (166+23/− 20, 299+235/− 133, 255+33/− 29 Ma; Table 2) could represent the end Paleozoic thermal event. The younging-upsection D1 path suggests that most of the apatite in this section is not recycled from the Late Cenozoic strata exposed south of the Kokshaal range. The observation that the hanging wall and footwall of the KBT have experienced a young episode of deformation and likely exhumation suggests that this region is the source area for the detrital sediments.

The procedure used to derive the average exhumation rate of a hinterland source from a population of thermochronologic data collected through a reasonably well-dated sedimentary sequence is discussed by Garver et al. [43]. Assuming a closure temperature of 105±5 °C (appropriate for the observed Cl content; [37]), a surface temperature of 10 °C, and a geothermal gradient of 22±3 °C/km (compatible with organic maturity studies and downhole temperatures from the southwest Tarim basin [19,44,45]) implies a closure depth of 3.3 to 5.6 km. Given the D1 lag time of 16 to 18 Ma, the long-term exhumation rate in the source area would be 0.2 to 0.3 mm/yr, although this has likely varied over time.

5. Discussion

We interpret the AFT ages from the hanging wall of the Maidan and Muziduke faults as reflecting thrust-driven exhumation beginning in the latest Oligocene–Early Miocene and continuing for at least several million years. The quality of the data do not conclusively show that the southern fault is the younger of the two, although this would be the predicted deformation pattern if we assume southward propagating deformation [46]. The pattern of faulting depicted in Fig. 2B suggests that Talas-Ferghana fault also became active at this time. There is no indication of another significant structure farther north within this range. At the longitude of this study, every major range within the Tian Shan north of the Kokshaal range has been investigated thermochronologically ([20,21,47]; Sobel, unpublished); none yield older Cenozoic reset cooling ages. South of the Muziduke fault, the only samples which yielded a reset AFT cooling age come from the hanging wall of the KBT and the Kuzigongsu section; the ages are early and middle Miocene, respectively. Other samples from Paleozoic and Mesozoic strata have experienced too little exhumation to be dated by AFT. The younger suite of FTGA from Miocene strata at Wenguri [19] and from Pliocene and younger sediment from the Boguzihe section yield ages around the Oligo-Miocene boundary. Therefore, we conclude that the Maidan fault zone represents the first significant contractile deformation in the Tian Shan at this longitude. Sediment derived from this exhumed region has likely provided a significant portion of the material deposited in the foreland basin to the south. The thrust belt propagated southward less than ca. 50 km between ca. 25 and 13 Ma.

The detrital grains preserved at the Wenguri section suggest moderately rapid exhumation in the source area between ca. 25 and 13 Ma; it is possible that the younger ages were derived from either the Kuzigongsu section, located to the west (Fig. 2A, [19]) or the hanging wall of the KBT to the north. The basal sample, with a minimum FTGA of ca. 25 Ma, was deposited at ca. 18 Ma [14], implying a lag time of ca. 7 Ma. The 3 to 0 Ma Boguzihe section yields minimum FTGA between ca. 21 and 16 Ma and lag times of 16 to 18 Ma. The similar age range and increasing lag times implies that relatively little bedrock exhumation occurred in the interval between 18 and 3 Ma. Indeed, the oldest Boguzihe ages suggest that the source area might have been rejuvenated during the Pliocene in the hanging wall of a southward propagating structure located to the north, such as the Keketamu fold or related structure. This agrees with the observation that the inferred source area, the hanging wall of the KBT, appears to have been recently deformed. The generally low relief of the study area despite the magnitude of exhumation required to expose reset AFT samples likely reflects the low erosional resistance of the sedimentary strata, particularly the Tertiary units.

Several attempts to estimate the onset of deformation in the Tian Shan have been made by dividing the total shortening across the range by the present shortening rate. Modern shortening rates across the entire range are estimated to be 19±3 mm/yr at 76°E and decrease to

4.7±1.5 mm/yr between 81 and 85°E and <1 mm/yr between 86 and 87°E (Fig. 1) [5–7]. As mentioned above, one such estimate at 76°E uses the ~200±50 km shortening estimate of Avouac et al. [8] with the 20 mm/yr GPS-derived shortening rate of Abdrakhmatov et al. [5] to infer that shortening initiated at ~ 10 Ma. However, no geologic cross-section has validated this total shortening across the range, and this method only accounts for deformation along the north and south margin of the Tian Shan, and not the intra-belt deformation [3], so this may represent minimum shortening values. Indeed, recognizing the uncertainty in this and other shortening estimates, Abdrakhmatov et al. [5] noted that deformation could have begun as early as 20–30 Myr or much more recently than 10 Ma. More recently, four preliminary magnetostratigraphic sections from the Kyrgyz portion of the Tian Shan, combined with structural studies, paleoseismology and GPS data have been interpreted as suggesting that the portion of the orogen north of the Kokshaal range, at approximately 76°E, experienced 35–80 km of shortening commencing at a slow rate at ca. 12 Ma and accelerating in the last 3–7 Ma [48]. Estimates have also been made for the Talas-Ferghana dextral fault, which crosscuts the range. Radiocarbon dating of geomorphic features offset across this fault suggest a Holocene slip rate of ~10 mm/yr; combined with estimates of no more than 100 km of Cenozoic slip, this suggests that the fault could have initiated within the last 10 Ma [31].

The discrepancy between the Late Oligocene–Miocene initiation of significant exhumation documented herein and the estimate of either a 10 Ma initiation predicted from geodetic measurements [5] or a 12 Ma initiation predicted from structural geology and stratigraphy [48] suggests that the Tian Shan at 76°E has undergone a complex Late Cenozoic shortening history. Indeed, Charreau et al. [11] showed that the sediment deposition rate in the northern Tarim basin at the Qiulitagh anticline (Fig. 1) doubled at 11 Myr; the authors attributed this to an acceleration of uplift and erosion of the Tian Shan at this time. It is possible that deformation along the southern margin of the Tian Shan has migrated south in distinct, pulsed events of heightened deformation on specific structures (KBT, MKBT, Keketamu Anticline, Atushi Anticline, Kashi Anticline), but these periods of deformation may be separated by periods of tectonic quiescence. Hence, the present day rate may represent a period of increased tectonic activity that is not indicative of the long-term average. Assuming that the present shortening rate could account for the total amount of Cenozoic shortening in 10 Ma and realizing that shortening initiated at least 15 Myr earlier, we conclude that the shortening rate must have increased over the last 10 Myr, although the exact timing is uncertain. A similar conclusion was reached by Reigber et al. [6]. The displacement history of the Talas-Ferghana fault likely has varied in a similar way.

Estimates of bulk crustal shortening (125 km at 84°E, 200 km at 76°E) as well as geodetically-determined shortening patterns show a westward-increasing orogen-normal shortening pattern [7,8]. This pattern has been interpreted as reflecting 7±2.5° clockwise rotation of the Tarim Block about a pole located at the eastern end of the range (~ 96°E) that commenced at 16+22/− 9 Ma [8,15]. To date, only 2 locations have yielded well-defined Oligo-Miocene cooling ages within the Tian Shan: Manas (Fig. 1, [18]) and the South Tian Shan (this study; [19]). Two additional localities within the interior of the range, between Kuqa and Manas (HP and YP, Fig. 1), yield poorly-defined Late Cenozoic cooling ages, associated with orogen-parallel strike-slip fault systems [20]. Seismic reflection data suggest a similar age for an angular unconformity in the subsurface south of Kuqa [16]. Two localities have yielded 10–11 Ma increases in sediment deposition rate, at Kuitun He [49] and the Qiulitagh anticline [11]; in addition, the Kyrgyz range began to be exhumed at ca. 11 Ma [21,47] (Fig. 1). Preliminary magnetostratigraphy data from the Kyrgyz Tian Shan suggest that sediment accumulation and hence deformation in this portion of the orogen commenced at ca. 12 Ma [48]. It seems difficult to reconcile the distribution of early-onset shortening localities with a simple rotational deformation model, although the distribution of Middle–Late Miocene data does agree well with this model. Therefore, we speculate that shortening within the Tian Shan initiated as orogen normal shortening during the latest Oligocene–Early Miocene; westward-increasing differential shortening driven by the rotation of the Tarim block became more pronounced around ~ 11–10 Myr with a rate that has likely increased during this period.

Acknowledgments

We thank Yin Jinhui, Nan Lin, Tian Qinjian, and Kate Scharer for their help with sample collection and Doug Burbank for thoughtful discussions. Funding was provided by the National Science Foundation of China Grants 403720081 and 49834005 and US National Science Foundation Grant EAR-0230403. Dieter Rhede and Oona Appelt helped collect the electron microprobe data. Jean-Philippe Avouac, Marc Jolivet, Stuart Gilder and an anonymous reviewer provided helpful critiques.

Appendix A. Supplementary data

Supplementary data associated with this article can be found, in the online version, at doi:10.1016/j.epsl.2006.03.048.

References

[1] D.W. Burbank, J.K. McLean, M. Bullen, K.Y. Abdrakhmatov, M.M. Miller, Partitioning of intermontane basins by thrust-related folding, Tien Shan, Kyrgyzstan, Basin Res. 11 (1) (1999).

[2] V.I. Bune, G.P. Gorshkov, Seismic Zoning Territory of the USSR. Methodical Bases and the Regional Description of the Map of 1978 Year, (Seismicheskoe rayonirovanie territorii SSSR. Metodicheskie osnovy I regionalnoe opisanie karty 1978 goda), Nauka, Moscow, 1980, p. 306 (in Russian).

[3] S.C. Thompson, R.J. Weldon, C.M. Rubin, K. Abdrakhmatov, P. Molnar, G.W. Berger, Late Quaternary slip rates across the central Tien Shan, Kyrgyzstan, central Asia, J. Geophys. Res., [Solid Earth] 107 (B9) (2002).

[4] P. Molnar, S. Ghose, Seismic moments of major earthquakes and the rate of shortening across the Tien Shan, Geophys. Res. Lett. 27 (2000) 2377–2380.

[5] K.Y. Abdrakhmatov, S.A. Aldazhanov, B.H. Hager, M.W. Hamburger, T.A. Herring, K.B. Kalabaev, K.B. Kalabayev, V.I. Makarov, P. Molnar, S.V. Panasyuk, M.T. Prilepin, R.E. Reilinger, I.S. Sadybakasov, B.J. Souter, Y.A. Trapeznikov, V. Y. Tsurkov, A.V. Zubovich, Relatively recent construction of the Tien Shan inferred from GPS measurements of present-day crustal deformation rates, Nature 384 (6608) (1996) 450–453.

[6] C. Reigber, G.W. Michel, R. Galas, D. Angermann, J. Klotz, J.Y. Chen, A. Papschev, R. Arslanov, V.E. Tzurkov, M.C. Ishanov, New space geodetic constraints on the distribution of deformation in Central Asia, Earth Planet. Sci. Lett. 191 (1-2) (2001) 157–165.

[7] Q. Wang, P.Z. Zhang, J.T. Freymueller, R. Bilham, K.M. Larson, X. Lai, X. You, Z. Niu, J. Wu, Y. Li, J. Liu, Z. Yang, Q. Chen, Present-day crustal deformation in China constrained by Global Positioning System measurements, Science 294 (2001) 574–577.

[8] J.P. Avouac, P. Tapponnier, M. Bai, H. You, G. Wang, Active thrusting and folding along the northern Tien Shan and late Cenozoic rotation of the Tarim relative to Dzungaria and Kazakhstan, J. Geophys. Res. 98 (4) (1993) 6755–6804.

[9] G.F. Sella, T.H. Dixon, A. Mao, REVEL: a model for Recent plate velocities from space geodesy, J. Geophys. Res. 31 (2002), doi:10.1029/2000JB000033.

[10] A. Yin, S. Nie, P. Craig, T.M. Harrison, F.J. Ryerson, X.L. Qian, G. Yang, Late Cenozoic tectonic evolution of the southern Chinese Tian Shan, Tectonics 7 (1) (1998) 1–27.

[11] J. Charreau, S. Gilder, Y. Chen, S. Dominguez, J.P. Avouac, S. Sen, M. Jolivet, Y. Li, W.M. Wang, Magnetostratigraphy of the Yaha section, Tarim Basin (China): 11 Ma acceleration in erosion and uplift of the Tianshan Mountains, Geology 34 (3) (2006) 181–184.

[12] J. Chen, D.W. Burbank, K.M. Scharer, E. Sobel, J. Yin, C. Rubin, R. Zhao, Magnetostratigraphy of the Pliocene–Pleistocene strata in the southwestern Chinese Tian Shan, and rates of Pleistocene folding and thrusting, Earth Planet. Sci. Lett. 195 (2002) 113–130.

[13] J. Chen, R. Heermance, D. Burbank, Late Cenozoic conglomerate progradation in the Southwestern Chinese Tian Shan: tectonic, climate or erosion control? Eos Trans. AGU, Fall Meet. Suppl., Abstract, vol. 85 (47), 2004, p. T53A-0472.

[14] R.V. Heermance, J. Chen, D.W. Burbank, E.R. Sobel, New age-constraints on syn-tectonic stratigraphy and basin evolution in the Southwestern Chinese Tian Shan foreland, AGU Fall meeting, Eos, Trans. AGU, San Francisco, 2005.

[15] F. Métivier, Y. Gaudemer, Mass transfer between eastern Tien Shan and adjacent basins (central Asia): constraints on regional tectonics and topography, Geophys. J. Int. 128 (1997) 1–17.

[16] D. He, J. Suppe, G. Yang, S. Guan, S. Huang, X. Shi, X. Wang, C. Zhang, Guidebook for fieldtrip in south and north Tianshan foreland basin, Xinjiang Uygur Autonomous region, China, International Conference on Theory and Application of Fault-related folding in Foreland Basins, 2005, p. 78, Beijing, China.

[17] E.R. Sobel, M.R. Strecker, Uplift, exhumation, and precipitation: Tectonic and climatic control of Late Cenozoic landscape evolution in the northern Sierras Pampeanas, Argentina, Basin Res. 15 (2003), doi:10.1046/j.1365-2117.2003.00214.x.

[18] M.S. Hendrix, T.A. Dumitru, S.A. Graham, Late Oligocene–Early Miocene unroofing in the Chinese Tian Shan: an early effect of the India-Asia collision, Geology 22 (1994) 487–490.

[19] E.R. Sobel, T.A. Dumitru, Exhumation of the margins of the western Tarim basin during the Himalayan orogeny, J. Geophys. Res. 102 (B3) (1997) 5043–5064.

[20] T.A. Dumitru, D. Zhou, E.Z. Chang, S.A. Graham, M.S. Hendrix, E.R. Sobel, A.R. Carroll, Uplift, exhumation, and deformation in the Chinese Tian Shan, in: M.S. Hendrix, G.A. Davis (Eds.), Paleozoic and Mesozoic Tectonic Evolution of Central and Eastern Asia: From Continental Assembly to Intracontinental Deformation, Memoir, vol. 194, Geological Society of America, Boulder, 2001, pp. 71–99.

[21] E.R. Sobel, M. Oskin, D. Burbank, A. Mikolaichuk, Exhumation of basement-cored uplifts: example of the Kyrgyz Range quantified with apatite fission-track thermochronology, Tectonics 25 (2006) TC2008, doi:10.1025/2005TC001809.

[22] A.R. Carroll, S.A. Graham, E. Chang, C.L. McKnight, Sinian through Permian tectonostratigraphic evolution of the northwestern Tarim basin, China, in: M.S. Hendrix, G.A. Davis (Eds.), Paleozoic and Mesozoic Tectonic Evolution of Central and Eastern Asia: From Continental Assembly to Intracontinental Deformation, Memoir, vol. 194, Geological Society of America, Boulder, 2001, pp. 47–70.

[23] M.L. Bazhenov, A.Q. Collins, K.E. Degtyarev, N.M. Levashova, A.V. Mikolaichuk, V.E. Pavlov, R. Van der Voo, Paleozoic northward drift of the North Tien Shan (Central Asia) as revealed by Ordovician and Carboniferous paleomagnetism, Tectonophysics 366 (2003) 113–141.

[24] Y.V. Khristov, A.V. Mikolaychuk, Geosynclinal basement of the crust of the Fergana-Kokshaal Hercynides, Geotectonics 17 (3) (1983) 233–241.

[25] M. Tagiri, T. Yano, A. Bakirov, T. Nakajina, S. Uchiumi, Mineral parageneses and metamorphic PT paths of ultrahigh-pressure eclogites from Kyrghyazstan Tien-Shan, Isl. Arc 4 (1995) 280–292.

[26] V.S. Burtman, Structural geology of Variscan Tien Shan, USSR, Am. J. Sci. 275-A (1975) 157–186.

[27] M.L. Bazhenov, V.S. Burtman, A.V. Dvorova, Permian paleomagnetism of the Tien Shan fold belt, Central Asia: post-collisional rotations and deformation, Tectonophysics 312 (2–4) (1999) 303–329.

[28] M.S. Hendrix, S.A. Graham, A.R. Carroll, E.R. Sobel, C.L. McKnight, B.J. Schulein, Z. Wang, Sedimentary record and climatic implications of recurrent deformation in the Tian Shan: evidence from Mesozoic strata of the north Tarim, south Junggar, and Turpan basins, Northwest China, Geol. Soc. Amer. Bull. 104 (1) (1992) 53–79.

[29] J. Chen, G. Ding, D.W. Burbank, K.M. Scharer, C. Rubin, E. Sobel, G. Qu, J. Shen, J. Yin, R. Zhao, Late Cenozoic Tectonics and Seismicity in the Southwestern Tian Shan, China, Earthq. Res. China 17 (2) (2001) 134–155.

[30] M.B. Allen, S.J. Vincent, P.J. Wheeler, Late Cenozoic tectonics of the Kepintage thrust zone: interactions of the Tien Shan and Tarim Basin, northwest China, Tectonics 18 (1999) 639–654.

[31] V.S. Burtman, S.F. Skobelev, P. Molnar, Late Cenozoic slip on the Talas-Ferghana fault, the Tien Shan, central Asia, Geol. Soc. Amer. Bull. 108 (1996) 1004–1021.

[32] Xinjiang Bureau of Geology and Mineral Resources, Regional geology of the Xinjiang Uygur Autonomous Region, Geological Publishing House, Beijing, 1993, 561 pp.

[33] E.R. Sobel, Basin analysis of the Jurassic–Lower Cretaceous southwest Tarim basin, NW China, Geol. Soc. Amer. Bull. 111 (5) (1999) 709–724.

[34] R.V. Heermance, J. Chen, K. Scharer, D. Burbank, Tertiary deformation in the Kashgar basin, southern margin of the Tian Shan, China Eos Tran. AGU 85 Fall Meet. Suppl., Abstract T31E-05, 2004.

[35] J. Chen, D.W. Burbank, K.M. Scharer, R. Heermance, C. Wang, Timing and Rates of Late Cenozoic Growth Folding in the Southwestern Chinese Tian Shan-Tarim Foreland Basin, 32nd International Geological Congress, Florence, Italy, 2004, p. 104-2.

[36] P.G. Fitzgerald, R.B. Sorkhabi, T.F. Redfield, E. Stump, Uplift and denudation of the central Alaska Range; a case study in the use of apatite fission track thermochronology to determine absolute uplift parameters, J. Geophys. Res. 100 (10) (1995) 20,175–20,191.

[37] R.A. Ketcham, R.A. Donelick, W.D. Carlson, Variability of apatite fission-track annealing kinetics: III. Extrapolation to geological time scales, Am. Mineral. 84 (9) (1999) 1235–1255.

[38] R.F. Galbraith, On statistical models for fission track counts, Math. Geol. 13 (1981) 471–478.

[39] P.F. Green, A new look at statistics in fission-track dating, Nucl. Tracks 5 (1981) 77–86.

[40] R.A. Donelick, R.A. Ketcham, W.D. Carlson, Variability of apatite fission-track annealing kinetics: II. Crystallographic orientation effects, Am. Mineral. 84 (9) (1999) 1224–1234.

[41] R.A. Ketcham, R.A. Donelick, M.B. Donelick, AFTSolve: a program for multi-kinetic modeling of apatite fission-track data, Geol. Mater. Res. 2 (1) (2000) 1–32.

[42] M.T. Brandon, Decomposition of mixed grain age distributions using binomfit, Track 24 (2002) 13–18.

[43] J.I. Garver, M.T. Brandon, M. Roden-Tice, P.J.J. Kamp, Exhumation history of orogenic highlands determined by detrital fission-track thermochronology, in: U. Ring, M.T. Brandon, G.S. Lister, S.D. Willett (Eds.), In Exhumation Processes: Normal Faulting, Ductile Flow and Erosion, vol. 154, Geological Society of London, 1999, pp. 283–304.

[44] S. Fan, Z. Zhou, C. Pan, L. Han, Y. Zhu, Paleotemperature and oil and gas of Tarim, Oil and Gas Geology of Tarim, Science Publishing House, Beijing, 1990, p. 77.

[45] H. Zhang, Geochemical Characteristics and Resource Prediction of Meso-Cenozoic Source Rocks in Tarim, 1989.

[46] 1 D. Davis, J. Suppe, F.A. Dahlen, Mechanics of fold-and-thrust belts and accretionary wedges, J. Geophys. Res. 88 (1983) 1153–1172.

[47] M.E. Bullen, D.W. Burbank, J.I. Garver, K.Y. Abdrakhmatov, Late Cenozoic tectonic evolution of the northwestern Tien Shan: new age estimates for the initiation of mountain building, Geol. Soc. Amer. Bull. 113 (12) (2001) 1544–1559.

[48] K.E. Abdrakhmatov, R. Weldon, S. Thompson, D. Burbank, C. Rubin, M. Miller, P. Molnar, Origin, direction, and rate of modern compression in the central Tien Shan, Kyrgyzstan, Geol. Geofiz. (Russ. Geol. Geophys.) 42 (2001) 1585–1609.

[49] J. Charreau, Y. Chen, S. Gilder, S. Dominguez, J.-P. Avouac, S. Sen, D. Sun, Y. Li, W.-M. Wang, Magnetostratigraphy and rock magnetism of the Neogene Kuitun He section (northwest China): implications for Late Cenozoic uplift of the Tianshan mountains, Earth Planet. Sci. Lett. 230 (2005) 177–192.

[50] K.M. Scharer, D.W. Burbank, J. Chen, R.J. Weldon, C. Rubin, R. Zhao, J. Shen, Detachment folding in the Southwestern Tian Shan-Tarim foreland, China: shortening estimates and rates, J. Struct. Geol. 26 (2004) 2119–2137.

[51] J. Thomas, H. Perroud, P.R. Cobbold, M.L. Bazhenov, V.S. Burtman, A. Chauvin, E. Sadybakasov, A paleomagnetic study of tertiary formations from the Kyrgyz Tien-Shan and its tectonic implications, J. Geophys. Res. 98 (B6) (1993) 9571–9589.

[52] A.J. Hurford, P.F. Green, The zeta age calibration of fission-track dating, Chem. Geol. 41 (4) (1983) 285–317.